Joint scheme for symbol, sampling clock, and carrier frequency synchronization in PDM-CO-OFDM system beyond 100 Gb/s

Zheng Yan (闫 峥)*, Yaochao Liu (刘耀超), and Xue Chen (陈 雪)

State Key Laboratory of Information Photonics and Optical Communications, Beijing University of Posts and Telecommunications, Beijing 100876, China

**Corresponding author: yanzhengbj@gmail.com*

Received March 17, 2014; accepted July 16, 2014; posted online September 26, 2014

We propose a joint scheme for symbol, sampling clock, and carrier frequency synchronization in a polarization division multiplexing coherent optical orthogonal frequency division multiplexing (PDM-CO-OFDM) system. Unlike other existing algorithms designed for specific impairment, the scheme can estimate and compensate for the interactional synchronization errors effectively without extra training overhead by building a comprehensive error model. The simulation shows that symbol synchronization error and sample timing error can be corrected by channel equalizer, and the estimation ranges of sampling frequency offset and normalized carrier frequency offset are about (–2000, 2000) ppm, and (–0.04 (–3.5), 0.04 (3.5)) Ghz, respectively.

OCIS codes: 060.0060, 060.1660, 060.2330.

doi: 10.3788/COL201412.100605.

The demand for large transmission capacity is increasing exponentially due to the rapid spread of global Internet services such as video sharing, cloud computing, and high-definition television. The high-speed optical transmission systems beyond 100 Gb/s have been actively investigated in the industrial field[1]. Because of its high spectral efficiency and flexibility, coherent optical orthogonal frequency division multiplexing (CO-OFDM), as one of the promising technologies, is employed in 400 Gb/s and 1 Tb/s systems[2,3]. However, the CO-OFDM transmission system is much vulnerable to the effects that destroy the orthogonality between subcarriers, such as symbol, sampling clock, and carrier frequency synchronizations. In order to avoid the inter-carrier interferences (ICI), the high accuracy of synchronization algorithms are indispensable to CO-OFDM. Recently, many algorithms have been proposed to solve different synchronization problems[4–8]. However, the existing algorithms are mostly designed for a specific impairment, and the interaction effects between the different impairments have not yet been considered. In practice, it is worth noting that the interaction effects will seriously deteriorate the system performance and should not be ignored.

In order to theoretically analyze the interaction effects between symbol synchronization error (SSE), sample timing error (STE), sampling frequency offset (SFO), and carrier frequency offset (CFO), we build a systematic mathematical model. Furthermore, a joint scheme for symbol, sampling clock, and carrier frequency synchronization is proposed to estimate and compensate for the mixed synchronization errors without extra training overhead in polarization-division multiplexing (PDM)-CO-OFDM systems beyond 100 Gb/s. Taking 480 Gb/s PDM-16 quadrature amplitude modulation (QAM) CO-OFDM system as an example, the joint scheme can not only avoid the interactions between different estimation algorithms but also achieve high estimation accuracy, fast convergence speed, and excellent compensation performance.

In the transmitter, the ith OFDM symbol $x_i(t)$ is shown as[9]

$$x_i(t) = \frac{1}{N}\sum_{k=0}^{N-1} S_i(k)\exp(\mathrm{j}2\pi kt/T)\ (i-1)\cdot T \le t \le i\cdot T, \quad (1)$$

where $S_i(k)$ represents the transmitted signal in the kth subcarrier of the ith OFDM symbol (i = 1, 2…, k = 0, 1, 2…N-1), N is the total subcarrier number of one OFDM symbol, T is the period of the OFDM symbol ($T = NT_s$), and T_s denotes the digital-to-analog converter (DAC) sampling period in the transmitter.

At the receiver of CO-OFDM system, the sampling clock mismatch between DAC and analog-to-digital converter (ADC) can introduce SFO and STE. After ADC, the mathematical model for the sampled signal $r_i(n)$ is shown as

$$\begin{aligned} r_i(n) &= h_i(t)\otimes x_i(t)\cdot\exp[-\mathrm{j}(2\pi\Delta f_c t+\Delta\phi_i)] + \eta_i(t)\,|_{t=(i-1)(N+N_{cp})T_s+nT_s+\Delta t_y} \\ &= h_i(n)\otimes\frac{1}{N}\sum_{k=0}^{N-1} S_i(\mathrm{k})\cdot\exp\{\mathrm{j}2\pi k[(i-1)(N+N_{cp})T_s+nT_s+\Delta t_y]/T\} \\ &\quad\times\exp\{-\mathrm{j}2\pi\Delta f_c[(i-1)(N+N_{cp})T_s+nT_s+\Delta t_y]-j\Delta\phi_i\}+\eta_i(n), \end{aligned} \quad (2)$$

 © 2014 Chinese Optics Letters

where $h_i(n)$ is the channel impulse response function in time domain, $\otimes$ represents convolution operation, N_{cp} is the number of cyclic prefix (CP), T_r is the ADC sampling period in the receiver, Δf_c is the CFO, $\Delta\phi_i$ is the phase impairment caused by laser linewidth, Δt_y is the STE, and $\eta_i(n)$ is the amplitude spontaneous emission (ASE) noise.

In general, the correlation of training symbols are utilized to complete symbol synchronization and CFO estimation[10–12]. The Schmidl algorithm is one of the typical algorithms for symbol synchronization and CFO estimation. In Schmidl algorithm, CFO is divided into fractional CFO (FCFO) and integer CFO (ICFO)[8,10,13–15]. Coarse symbol synchronization and FCFO estimation are completed in time domain. Because of the influence of ASE noise and inter symbol interference (ISI) caused by polarization mode dispersion (PMD) and chromatic dispersion (CD), the coarse symbol synchronization and FCFO estimation will induce SSE and residual CFO (RCFO)[8,16,17]. The SSE will bring about linear phase impairment in different subcarriers after the process of fast Fourier transformation (FFT), and RCFO will also induce the same phase impairment in all the subcarriers of one OFDM symbol. Besides, ICFO will lead to a cyclic shift between different subcarriers which can also be compensated for in Schmidl algorithm. After FFT and ICFO compensation, the sampled signal in frequency domain which includes the impairments caused by SSE, STE, SFO, RCFO, and laser linewidth is described as

$$R_i(k) = S_i(k)H_i(k)\underbrace{\frac{1}{N}\frac{\sin\left(\pi N\left(\frac{k}{N}\frac{\Delta T_s}{T_s}-\Delta e T_s\right)\right)}{\sin\left(\pi\left(\frac{k}{N}\frac{\Delta T_s}{T_s}-\Delta e T_s\right)\right)}}_{C(k)} \times \exp\left(\underbrace{\mathrm{j}2\pi k(i-1)\left(1+\frac{N_{cp}}{N}\right)\frac{\Delta T_s}{T_s}-\mathrm{j}2\pi\Delta e(i-1)(N+N_{cp})T_s}_{\varphi_i(k)} + \underbrace{\frac{\mathrm{j}\pi(N-1)k}{N}\frac{\Delta T_s}{T_s}-\mathrm{j}\pi(N-1)\Delta e T_s+\frac{\mathrm{j}2\pi k}{N}\frac{\Delta t_y+\Delta t_f}{T_s}-\mathrm{j}\Delta\phi_i}_{\phi(k)}\right)+\mathrm{ICI}_i(k)+\eta_i(k), \quad (3)$$

where $R_i(k)$ denotes the kth subcarrier in the ith OFDM symbol in the receiver, $H_i(k)$ represents the frequency-domain channel response, $\mathrm{ICI}_i(k)$ is the ICI, $\eta_i(k)$ is the ASE noise, ΔT_S is the SFO, $\Delta T_S = T_r - T_s$, Δe is the RCFO, and Δt_y and Δt_f are STE and SSE, respectively. There are three kinds of impairments induced by different synchronization errors: 1) amplitude impairment $C(k)$, which is caused by SFO and RCFO, 2) phase impairment $\varphi_i(k)$ and $\phi(k)$, where $\varphi_i(k)$ relies on the OFDM symbol ordinal number i, and $\phi(k)$ is the same between adjacent symbols, and 3) ICI impairment.

Generally, the amplitude impairment can be easily compensated for in channel equalization. However, the phase impairments caused by different synchronization errors are mixed together. In practice, it is almost impossible to estimate and compensate for a certain synchronization error accurately without considering the interaction effects between SSE, STE, SFO, and RCFO. Therefore, a joint synchronization scheme considering all the synchronization errors is proposed for the PDM-CO-OFDM system.

In the joint scheme, the traditional Schmidl algorithm is utilized to complete coarse symbol synchronization and CFO estimation. The phase impairments caused by SSE and STE are designed to be compensated for in channel equalization. An algorithm is proposed to estimate SFO and RCFO simultaneously by reusing the channel training sequences and pilots. The estimation results of SFO and RCFO are fed back to time domain to correct the sampling clock frequency by using interpolation filter and compensate for the phase impairment caused by RCFO, respectively. Figure 1 shows the digital signal processing (DSP) structure of the proposed joint synchronization scheme.

To correct the effects of SFO on the received digital signal, we utilize a polynomial-based interpolation filter in time domain to resample the digital signals according to the feedback parameter SFO[15]. To reduce the overhead of CP, the overlapped frequency-domain equalizer is employed to compensate for the CD-induced impairment, and the algorithm will not be influenced by synchronization errors because the compensation coefficients in frequency domain are already known[2,8,14]. Then, the traditional Schmidl algorithm is applied to complete coarse symbol synchronization

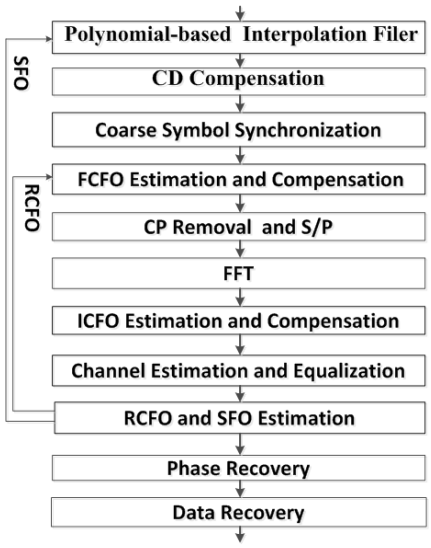

Fig. 1. DSP structure of the proposed synchronization scheme.

and estimate FCFO in time domain. Because of the influence of ASE noise and ISI caused by PMD and CD, the coarse symbol synchronization and FCFO estimation will induce SSE and RCFO. After CP removal, series-to-parallel conversion, and FFT, the digital signal is transformed into frequency domain after which the ICFO is estimated and compensated for. The estimation and compensation of ICFO are also based on traditional Schmidl algorithm. In frequency domain, the existing synchronization errors, such as SSE, STE, SFO, and RCFO, will induce mixed phase impairments to the sampled signal in the receiver. In the channel estimation and compensation module, the channel impulse response will be estimated and compensated for by using channel training sequences. Besides, we also find that the estimated channel impulse response contains the phase impairment caused by SSE and STE, and the phase impairment will be compensated for in channel equalization, the mechanism of which will be fully demonstrated below. After the phase impairments caused by SSE and STE are corrected, RCFO and SFO are estimated by reusing channel training symbols and pilots. The estimated results of RCFO and SFO are fed back to the FCFO compensation module and interpolation filter module to compensate for the FCFO and resample the digital signal in time domain, respectively. After several times of feedback processing, the closed loop will achieve convergence state and the SSE, STE, SFO, and CFO will be fully corrected. Finally, the phase impairment caused by laser linewidth will be compensated for in the phase recovery module by using the pilot subcarriers[13].

In PDM-CO-OFDM system, the received digital signal in frequency domain which contains the synchronization errors such SSE, STE, SFO, and RCFO can be described as

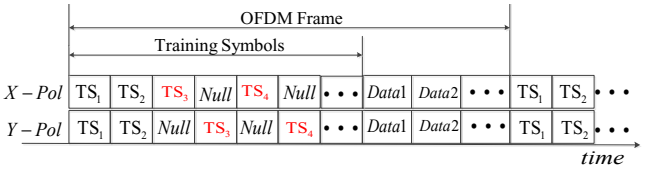

Fig. 2. Structure of channel training sequence.

$$\begin{bmatrix} R_{i,X}(k) \\ R_{i,Y}(k) \end{bmatrix} = \begin{bmatrix} H_{i,xx}(k) & H_{i,xy}(k) \\ H_{i,yx}(k) & H_{i,yy}(k) \end{bmatrix} \bullet \begin{bmatrix} S_{i,X}(k)C(k)e^{j\phi(k)}e^{j\varphi_i(k)} + \eta_{i,X}(k) \\ S_{i,Y}(k)C(k)e^{j\phi(k)}e^{j\varphi_i(k)} + \eta_{i,Y}(k) \end{bmatrix}, \quad (4)$$

where X and Y denote the polarization states, $H_{i,xx}(k)$, $H_{i,yx}(k)$, $H_{i,xy}(k)$, and $H_{i,yy}(k)$ are the channel frequncy-domain responses of the kth subcarrier in the ith symbol. $C(k)$, $\phi(k)$, and $\varphi_i(k)$ have the same meanings as in Eq. (3), and $\eta_{i,X(Y)}(k)$ is the sum of ICI and ASE noise. A piece of known training symbol is inserted periodically in the symbol stream for channel estimation[4]. Figure 2 shows the structure of the channel training sequence used in PDM-CO-OFDM system. Training symbols, TS_1 and TS_2, are used for coarse synchronization and CFO estimation; the training symbols TS_3 and TS_4 are used for channel estimation.

By using the training symbols, the frequency-domain channel matrix can be estimated. Taking the estimation of $H_{i,xx}(k)$as an example, the estimation result of $H_{i,xx}(k)$ can be described as

$$\tilde{H}_{i,xx}(k) = \frac{R_{i,X}(k)}{S_{i,X}(k)} = H_{i,xx}(k)C(k)e^{j\phi(k)}e^{j\varphi_i(k)} + \frac{H_{i,xx}(k)\eta_{i,X}(k) + H_{i,xy}(k)\eta_{i,Y}(k)}{S_{i,X}(k)}. \quad (5)$$

In order to eliminate the effect of ICI and ASE noise on the accuracy of the estimation result, an average operation is necessary. The average estimated channel matrix can be denoted as

$$\begin{bmatrix} \tilde{H}_{xx}(k) & \tilde{H}_{xy}(k) \\ \tilde{H}_{yx}(k) & \tilde{H}_{yy}(k) \end{bmatrix} \approx \begin{bmatrix} H_{xx}(k)C(k)e^{j\phi(k)}e^{j\theta(k)} & H_{xy}(k)C(k)e^{j\phi(k)}e^{j\theta(k)} \\ H_{yx}(k)C(k)e^{j\phi(k)}e^{j\theta(k)} & H_{yy}(k)C(k)e^{j\phi(k)}e^{j\theta(k)} \end{bmatrix}, \quad (6)$$

$$\theta(k) = 2\pi k\left(1 + \frac{N_{cp}}{N}\right)\frac{\Delta T_s}{T_s}(N_{TS} - 1) - 2\pi\Delta f_c (N + N_{cp})T_s(N_{TS} - 1), \quad (7)$$

where N_{TS} is the number of channel training symbols, and $\tilde{H}_{xx}(k)$, $\tilde{H}_{xy}(k)$, $\tilde{H}_{yx}(k)$, and $\tilde{H}_{yy}(k)$ are the mean values of the frequency-domain channel response, which contains phase cumulative term $\theta(k)$.

The digital signal in frequency domain after channel equalization can be denoted as

$$\begin{bmatrix} \tilde{S}_{i,X}(k) \\ \tilde{S}_{i,Y}(k) \end{bmatrix} = \begin{bmatrix} \tilde{H}_{xx}(k) & \tilde{H}_{xy}(k) \\ \tilde{H}_{yx}(k) & \tilde{H}_{yy}(k) \end{bmatrix}^{+} \bullet \begin{bmatrix} R_{i,X}(k) \\ R_{i,Y}(k) \end{bmatrix} = \begin{bmatrix} S_{i,X}(k)\exp[\mathrm{j}\varphi_i(k) - \mathrm{j}\theta(k)] + \eta_{i,X}(k) \\ S_{i,Y}(k)\exp[\mathrm{j}\varphi_i(k) - \mathrm{j}\theta(k)] + \eta_{i,Y}(k) \end{bmatrix}$$

$$= \begin{bmatrix} S_{i,X}(k)\exp\left(\mathrm{j}2\pi k(1+\frac{N_{cp}}{N})(i-N_{TS}+1)\frac{\Delta T_s}{T_s} - \mathrm{j}2\pi\Delta e(i-N_{TS}+1)(N+N_{cp})T_s - \mathrm{j}\Delta\phi_i\right) + \eta_{i,X}(k) \\ S_{i,Y}(k)\exp\left(\mathrm{j}2\pi k(1+\frac{N_{cp}}{N})(i-N_{TS}+1)\frac{\Delta T_s}{T_s} - \mathrm{j}2\pi\Delta e(i-N_{TS}+1)(N+N_{cp})T_s - \mathrm{j}\Delta\phi_i\right) + \eta_{i,Y}(k) \end{bmatrix}, \quad (8)$$

where $\tilde{S}_{i,X}(k)$ and $\tilde{S}_{i,Y}(k)$ are the frequency-domain digital signal after channel equalization in X and Y polarization states, respectively and $[\cdot]^{+}$ denotes matrix inverse operation. From Eq. (8), we know that the phase impairment caused by SSE and STE can be compensated for completely in the processing of channel equalization and the remaining phase impairment only contains the phase impairment caused by SFO and RCFO.

In the scheme, the channel training symbols are equalized by using the estimated channel matrix, and the equalized training symbols and pilots in data symbols are also reused to estimate RCFO and SFO. The processing structure of the estimation algorithm is shown in Fig. 3. The kth subcarrier in the $(i + \Delta i)$th symbol is multiplied by the conjugation of the kth subcarrier in the ith symbol. Similarly, the $(-k)$th subcarrier will also be processed in the same way. The phases of the processing results are extracted to estimate the normalized RCFO and SFO which can be denoted as $\Delta\hat{e}/f_s$ and $\Delta\hat{T}_s/T_s$, respectively. $f_s = 1/T_s$ is the ideal sampling clock frequency in the transmitter. The extracted phase can be denoted as

$$\xi(k) = \mathrm{angle}\left(\frac{\tilde{S}_{i+\Delta i,X}(k)}{\tilde{S}_{i,X}(k)}\right) \approx 2\pi\Delta i\left(1+\frac{N_{cp}}{N}\right)\frac{\Delta T_s}{T_s}k - 2\pi\Delta e\Delta i(N+N_{cp})T_s, \quad (9)$$

where Δi is the training symbol step length.

From Eq. (9), the estimation of RCFO and SFO can be obtained as

$$\begin{cases} \Delta\hat{e}/f_s = -\dfrac{\xi(k)+\xi(-k)}{4\pi\Delta i(N+N_{cp})} \\ \Delta\hat{T}_s/T_s = \dfrac{\xi(k)-\xi(-k)}{4\pi k\Delta i(1+N_{cp}/N)} \end{cases}. \quad (10)$$

By using a moving window which contains training symbols and pilots, the noise can be eliminated from the SFO and RCFO estimation result. Then, the estimated SFO and RCFO are fed back to time domain to correct the sampling clock and FCFO. In the interpolation filter module, we choose polynomial-based interpolation filter to resample the digital signal. The polynomial-based interpolation filter can correct the influence of the unsynchronized sampling clock, and its performance is better than the Lagrange interpolation filter[15].

The performance of the proposed scheme is simulated in 480 Gb/s PDM-16QAM CO-OFDM system built in VPI Transmission Maker 8.5 and MATLAB (shown in Fig. 4). In the simulation platform, the generation of the transmitted signal and the DSP in the receiver are completed in MATLAB, and the optical transmitter, optical fiber, and optical receiver are built in VPI Transmission Maker 8.5. The bit rate and baud rate in each polarization are 240 Gb/s and 60 Gbaud, respectively. In the transmitter, the pseudorandom bit sequence with a length of 2^{15}-1 as the transmitted data stream is mapped to the 16-QAM constellation which will be modulated to the middle 72 subcarriers of one OFDM symbol. The signals generated in frequency domain are converted into time domain after inverse FFT with the size of 128. Eight pilots are inserted into the middle 72 subcarriers symmetrically for phase recovery, and the other 48 subcarriers are padded with zero

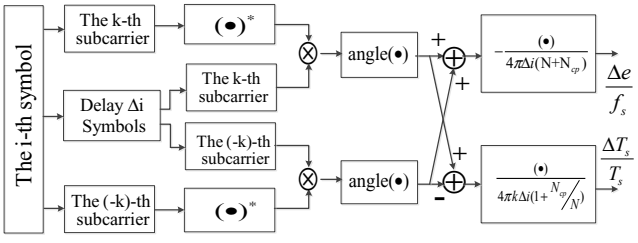

Fig. 3. Estimation algorithm for SFO and RCFO.

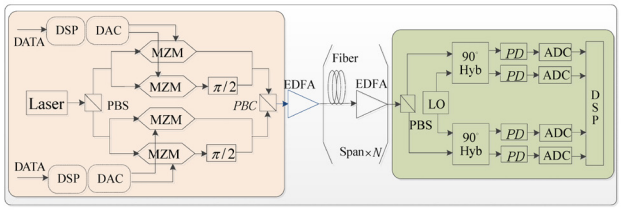

Fig. 4. Setup of the 480 Gb/s PDM-OFDM-16QAM system.

Table 1. Parameters of Fiber Link in VPI Transmission Maker

Attenuation (dB/km)	Dispersion (ps/km/nm)	PMD (ps/km$^{1/2}$)	Nonlinear Index ($W^{-1}km^{-1}$)	Effective Area (μm^2)	EDFA Gain (dB)	Noise Figure (dB)
0.20	20	0.5	1.16	80	16	4

for oversampling. Fourteen CPs are added to the head and the tail of each OFDM symbol as guard intervals, respectively. Figure 2 shows the OFDM frame transmitted in the simulation platform. The former two training symbols are used for coarse synchronization and CFO estimation. The following 60 channel training symbols are used for the estimation of channel impulse response, and data symbols follow the training symbols. In the transmission system, forward error correction is not employed. After the OFDM-baseband signals are generated in DSP modules, the real and imaginary parts of the OFDM signals are converted into analog signals by DACs with the sampling rate of 96 GS/s. The subcarrier spacing of the CO-OFDM signal is 750 MHz. The analog signals are used to drive the two Mach–Zehnder modulators to generate the modulated optical signals. The center frequency and the linewidth of the laser are 193.1 THz and 100 kHz, respectively. The optical signals in two polarizations are converged into the fiber channel through a polarization beam combiner.

An erbium-doped fiber amplifier (EDFA) is employed to control the launch power of the optical signal to be 2 dBm which is not to be optimized. The standard single-mode fiber, 12 spans in total and each span 80 km, is used in the simulation, and the parameters of the fiber link is shown in Table 1. The power attenuation of 16 dB after each span is fully compensated for by an EDFA with 4 dB noise. At the receiver, the optical signal is divided into two polarizations through a polarization beam splitter. The optical signals are converted into electrical domain by utilizing CO receivers. Four ADCs with 8 bit of resolution at 96 GS/s are utilized to sample the electrical signals, and the discrete samples are stored for DSP.

From Eq. (3), we know that SSE and STE have a similar influence on the received signal, and the ranges of SSE and STE are ±1/2CP length and ±1/2 sampling period, respectively. The compensation performance of SSE and STE in channel equalization is verified when only SSE and STE exist in the simulation. Figure 5 shows the constellation diagram before and after the channel equalization. From Figs. 5(a) and (b), we come to a conclusion that the channel equalization can be successfully compensated for the phase impairment caused by SSE and STE, and specific algorithms for SSE and STE estimation are not necessary in the scheme.

The extracted phase in Eq. (9) is utilized to estimate RCFO and SFO, and the algorithm will not work if the phase $\xi(k)$ is out of the range of $(-\pi, \pi)$. From the analysis, the estimation range of SFO and RCFO is shown in Fig. 6(a). The x-axis and y-axis denote the RCFO and the SFO both normalized by sampling rate f_s, respectively, and the four curves with different colors denote different estimation ranges with the changing of estimated symbol step Δi. If the values of SFO and RCFO are in the inner area of the closed curve with the same color, the estimation algorithm shown in Eqs. (9) and (10) will work normally because the total phase caused by SFO and RCFO is in the range of $(-\pi, \pi)$. It can be seen that the larger estimation range can be obtained if smaller symbol step Δi is chosen. Notice that channel estimation training sequences come in pairs which make the value of Δi to be a multiple of 2. To compare the performances of the proposed joint scheme and independent compensation scheme, the independent compensation scheme with SFO compensation algorithm[6] and CFO estimation algorithm[8] is simulated. In the simulation, SFO and CFO are 100 ppm and 3.5 GHz, respectively. From Fig. 6(b) we know that the bit error rate (BER) of the independent compensation scheme is close to 0.5, it means that the independent synchronization algorithm does not work normally. Consequently, a joint synchronization scheme is necessary to estimate and compensate for the interactional synchronization impairments. The performance of the proposed joint scheme is fully demonstrated in the following simulation.

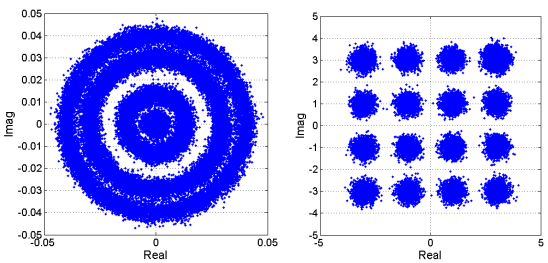

(a) (b)

Fig. 5. (a) Constellation diagram without SSE and STE compensated and (b) constellation diagram after channel equalization.

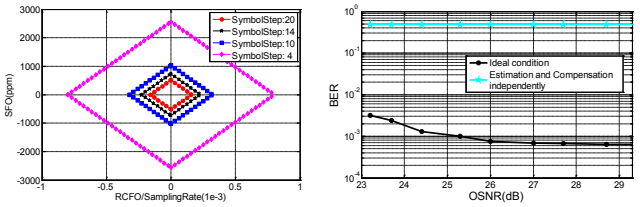

Fig. 6 (a) Estimation range of SFO and RCFO and (b) BER curve versus OSNR.

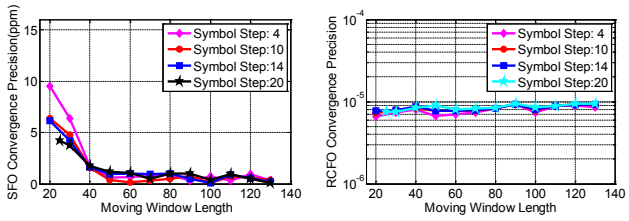

(a) (b)

Fig. 7 (a) SFO and (b) RCFO convergence precision curve versus moving window length.

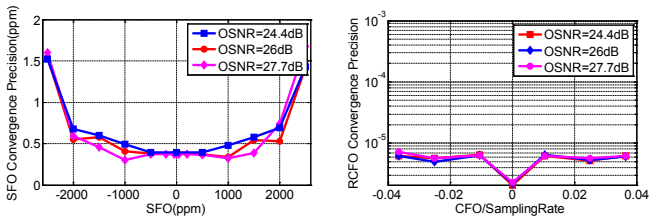

(a) (b)

Fig. 9. Convergence precision as a function of (a) SFO and (b) normalized CFO.

Generally, the estimation accuracy of SFO and RCFO is related to the estimated symbol step length Δi and the moving window length. In the simulation, we induce 3.5 GHz CFO and 500 ppm SFO, optical signal-to-noise ratio (OSNR) is 26 dB, and other conditions are fully described in the parameter part. Figure 7 shows the convergence precision of SFO and RCFO as a function of the moving window length with different symbol step lengths. It can be seen from Fig. 7(a), that the SFO convergence precision is improved with the increase in moving window length. The RCFO convergence precision will not change with the increasing window length (Fig. 7(b)). Besides, the convergence precision curves are almost the same in condition of different symbol steps, and the final estimation error is invariant after 60 estimated symbols, which does not impact BER performance. To obtain high convergence precision and large estimation range, the moving window length and the symbol step for SFO and RCFO estimations are chosen as 60 and 4, respectively, in the following simulation.

In the scheme, the estimated SFO and RCFO are fed back to time domain to correct the sampling clock and compensate for the FCFO, respectively. After several closed-loop processing times, the SFO and RCFO can be limited to the required accuracy range and the whole structure can come to the state of convergence. In the simulation, the CFO is 3.5 GHz, OSNR is 26 dB, and other conditions are the same which are described in the parameter part. Figure 8 shows the SFO and RCFO convergence precision as a function of the moving window processing number in condition of different SFOs. From the simulation, we come to a conclusion that the closed loop can be achieved at the convergence state after four times moving window processing, and the SFO and RCFO convergence precisions can reach 0.5 ppm and 5×10^{-5} normalized by sampling rate, respectively, whose influence for BER can be ignored.

To obtain the maximum processing range of SFO and RCFO, we investigated how the SFO and RCFO convergence precisions change with SFO and CFO. Figure 9 shows the SFO and RCFO convergence precisions as the functions of SFO and CFO, respectively. Figure 9(a) shows that SFO estimation range can reach up to (–2000, 2000 ppm), and the convergence precision of SFO can be 0.5 ppm. Figure 9(b) shows that the normalized CFO processing range can reach up to (–0.04, 0.04) (corresponding to the absolute CFO range [–3.5, 3.5 GHz]), and the normalized estimation accuracy is 5×10^{-5}. Besides, the convergence performance will stay the same when OSNR changes, which proves that the estimation algorithm has strong tolerance to OSNR.

Finally, we discuss how OSNR affects the SFO convergence precision and BER performance. The simulation condition: CFO is 3.5 GHz and other conditions are the same which are described in the parameter part. Figure 10(a) shows the SFO convergence precision curve versus OSNR with different induced SFOs. The variety of OSNR almost does not have bad effect on the estimation precision, and SFO convergence precision is limited to 1 ppm in condition of different SFOs which will not impact BER performance. Figure 10(b) shows the BER curve when the closed loop is convergent versus OSNR in condition of different SFOs. It can be seen from Fig. 10(b) that the BER performance is improved with the increasing OSNR, and will not change much with the increasing SFO. The BER platform in Fig. 10(b) is caused by nonlinear effect which is not compensated for in the DSP

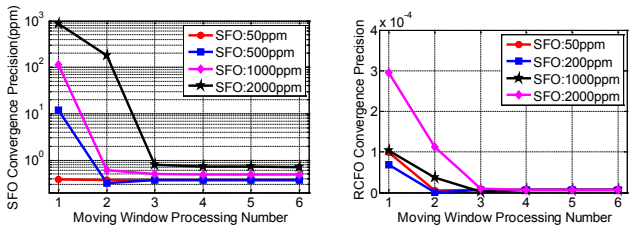

(a) (b)

Fig. 8. (a) SFO and (b) RCFO estimation error curve versus moving window number.

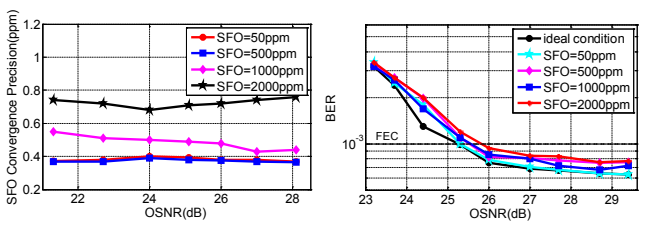

(a) (b)

Fig. 10. (a) SFO estimation precision curve versus OSNR and (b) BER curve versus OSNR.

module. The platform will disappear when the nonlinear effect is closed in the VPI Transmission Maker. Compared with ideal condition, the OSNR should be 25.2 dB at least to achieve the BER 1×10^{-3}, and less than 0.5 dB penalty is induced when the SFO is 2000 ppm.

In conclusion, we propose a joint synchronization scheme for SSE, STE, SFO, and CFO in the high-speed CO-OFDM system, and the performance is fully simulated in 480 Gb/s PDM-16QAM CO-OFDM system. The simulation shows that the scheme can successfully track ±0.04 (±3.5 GHz) normalized CFO and ±2000 ppm SFO in poor OSNR condition by reusing the channel estimation training sequences and pilots. The convergence precisions of CFO and SFO are 5×10^{-5} and 0.5 ppm, respectively. Meanwhile, the SSE and STE can be eliminated based on the fact that channel equalization can compensate for the phase impairment caused by SSE and STE, which can avoid specific estimation algorithm for SSE and STE. Besides, the whole closed-loop structure can correct the interactional synchronization errors and achieve excellent BER performance with fast convergence speed, no extra training overhead and OSNR penalty compared with the system with ideal condition.

This work was supported by the National 863 Program of China (No. 2012AA011303) and the Fund of Sate Key Laboratory of Information Photonics and Optical Communications (Beijing University of Posts and Telecommunications), China.

References

1. E. Ip, P. Ji, E. Mateo, Y. Huang, L. Xu, D. Qian, N. Bai, and T. Wang Proc. IEEE **100,** 1065 (2012).
2. X. Liu, S. Chandrasekhar, B. Zhu, P. J. Winzer, A. H. Gnauck, and D. W. Peckham, J. Lightwave Technol. **29,** 483 (2011).
3. C. Li, M. Luo, X. Xiao, J. Li, Z. He, Q. Yang, Z. Yang, and S. Yu, Chin. Opt. Lett. **12,** 040601 (2014).
4. S. L. Jansen, I. Morita, T. C. Schenk, and H. Tanaka, J. Opt. Netw. **7,** 73 (2008).
5. Y. Qiao, Z. Wang, and Y. Ji, Chin. Opt. Lett. **8,** 888 (2010).
6. X. Yi and K. Qiu, Opt. Express **19,** 13503 (2011).
7. C. J. Youn, X. Liu, S. Chandrasekhar, Y. H. Kwon, J. H. Kim, J. S. Choe, D. J. Kim, K. S. Choi, and E. S. Nam, Opt. Express **19,** 16174 (2011).
8. X. Zhou, K. Long, R. Li, X. Yang, and Z. Zhang, Opt. Express **20,** 7350 (2012).
9. J. Armstrong, J. Lightwave Technol. **27,** 189 (2009).
10. T. M. Schmidl and D. C. Cox, IEEE Trans. Commun. **45,** 1613 (1997).
11. K. Shi and E. Serpedin, IEEE Trans. Wireless Commun. **3,** 1271 (2004).
12. H. Minn, V. K. Bhargava, and K. B. Letaief, IEEE Trans. Wireless Commun. **2,** 822 (2003).
13. Y. Xingwen, W. Shieh, and T. Yan, IEEE Photon. Technol. Lett. **19,** 919 (2007).
14. R. Kudo, T. Kobayashi, K. Ishihara, Y. Takatori, A. Sano, and Y. Miyamoto. J. Lightwave Technol. **27,** 3721 (2009).
15. J. Vesma and T. Saramaki, Circuits Syst. Signal Process. **26,** 115 (2007).
16. W. Shieh, X. Yi, Y. Ma, and Q. Yang, J. Opt. Netw. **7,** 234 (2008).
17. Y. Huang, X. Zhang, and L. Xi, J. Opt. Commun. Netw. **5,** 584 (2013).